Towards quantum computing for the classical $O(2)$ model

Haiyuan Zou[1], Yuzhi Liu[2], Chen-Yen Lai[3], J. Unmuth-Yockey[1], A. Bazavov[1,3], Z. Y. Xie[4], T. Xiang[4], S. Chandrasekharan[5], S.-W. Tsai[3], and Y. Meurice[1]

[1] *Department of Physics and Astronomy, The University of Iowa, Iowa City, Iowa 52242, USA*
[2] *Department of Physics, University of Colorado, Boulder, Colorado 80309, USA*
[3] *Department of Physics and Astronomy, University of California, Riverside, CA 92521, USA*
[4] *Institute of Physics, Chinese Academy of Sciences, P.O. Box 603, Beijing 100190, China and*
[5] *Department of Physics, Duke University, Durham, NC 27708, USA*

(Dated: March 21, 2014)

We construct a sequence of steps connecting the classical $O(2)$ model in 1+1 dimensions, a model having common features with those considered in lattice gauge theory, to physical models potentially implementable on optical lattices and evolving at physical time. We show that the tensor renormalization group formulation of the classical model allows reliable calculations of the largest eigenvalues of the transfer matrix. We take the time continuum limit and check that finite dimensional projections used in recent proposals for quantum simulators provide controllable approximations of the original model. We propose two-species Bose-Hubbard models corresponding to these finite dimensional projections at strong coupling and discuss their possible implementations on optical lattices. The full completion of this program would provide a proof of principle that quantum computing is possible for classical lattice models.

PACS numbers: 05.10.Cc, 11.15.Ha, 37.10.Jk, 67.85.Hj, 75.10.Hk

arXiv:1403.5238v1 [hep-lat] 20 Mar 2014

Recently, there has been a lot of interest in the possibility of building quantum simulators using optical lattices [1–5]. The goal is to engineer many-body systems with cold atoms that can be built experimentally and that evolve according to a quantum Hamiltonian that approximately corresponds to theoretical models studied in condensed matter or lattice gauge theory (LGT). We call this new approach of theoretical models "quantum computing". In the following, we focus on the needs of LGT where quantum simulators would allow us to deal with the sign problem of Quantum Chromodynamics with a chemical potential and to study real time evolution.

Lattice gauge theories were initially developed in the Hamiltonian formulation [6–9] using local gauge variables that live on bonds connecting neighboring sites. These gauge links are operators that live on an infinite Hilbert space and in the appropriate basis look like classical group elements. For example, in $U(1)$ LGT [7], gauge links are phases $e^{i\theta}$, which when considered as operators, live in an infinite dimensional Hilbert space spanned by the eigenstates $|n\rangle$ of the "angular momentum" operator $L = -i\partial/\partial\theta$ with all positive and negative integer eigenvalues n.

For realistic implementations with cold atoms, it is convenient to consider Hamiltonians where gauge links are quantum operators that live in a finite rather than infinite Hilbert space [10, 11]. In the $U(1)$ example this would mean the eigenvalues of L only take a finite range of values. For this to occur naturally one restricts the Hilbert space to be in a spin-s representation, i.e., $n = -s, -(s-1), ..0, ..(s-1), s$, with L replaced by L^3, the third component of the usual angular momentum algebra, while the operators corresponding to $e^{\pm i\theta}$ become $L^{\pm}$.

Such quantum link variables have played an important role in several proposals to simulate dynamical gauge fields on optical lattices [1–3]. In this Letter, we use new numerical methods [12–15] to show that the restricted Hilbert space of the quantum link model can controllably reproduce important features of the original classical model and provide an explicit connection with quantum models implementable on optical lattices. The model considered is the classical $O(2)$ model in 1+1 dimensions with a chemical potential μ [16]. This is the simplest, nontrivial, model where Abelian, quantum link inspired, projections can be introduced. If $\mu \neq 0$, the action is complex and Monte Carlo methods suffer from a sign problem. However, the tensor renormalization group (TRG) method [12, 13, 15] allows us to deal efficiently with sign problems [14] and can be checked with the worm algorithm [17, 18] when μ is real. The TRG also allows us to take the time continuum limit and connect to the Hamiltonian formalism and Bose-Hubbard models [19–21].

The partition function of the model considered here reads

$$Z = \int \prod_{(x,t)} \frac{d\theta_{(x,t)}}{2\pi} e^{-S} \ , \tag{1}$$

with action

$$\begin{aligned} S = &- \beta_t \sum_{(x,t)} \cos(\theta_{(x,t+1)} - \theta_{(x,t)} - i\mu) \\ &- \beta_x \sum_{(x,t)} \cos(\theta_{(x+1,t)} - \theta_{(x,t)}). \end{aligned} \tag{2}$$

The sites of the rectangular $N_x \times N_t$ lattice are labeled as (x,t) and we assume periodic boundary conditions in

space and time. When $\beta_t \gg \beta_x$ we obtain the time continuum limit [8, 9, 22] with an Hamiltonian connecting quantum rotors on a lattice with β_x acting as the coupling between the spatial sites:

$$\hat{H} = \frac{\tilde{U}}{2} \sum_x \hat{L}_x^2 - \tilde{\mu} \sum_x \hat{L}_x - \tilde{J} \sum_{\langle xy \rangle} \cos(\hat{\theta}_x - \hat{\theta}_y) \ , \quad (3)$$

with $\tilde{U} = 1/(\beta_t a)$, $\tilde{\mu} = \mu/a$ and $\tilde{J} = \beta_x/a$, the sum extending over sites x and nearest neighbors $\langle xy \rangle$ of the space lattice and a is a lattice spacing.

The commutation relations $[L, \mathrm{e}^{\pm i\hat{\theta}}] = \pm \mathrm{e}^{\pm i\hat{\theta}}$ suggest that $\mathrm{e}^{\pm i\hat{\theta}}$ are creation and annihilation operators. However, there is no eigenstate of L annihilated by $\mathrm{e}^{-i\hat{\theta}}$. At large μ, there is an effective truncation [23, 24] which makes the eigenstates with negative eigenvalues irrelevant. For small value of μ, we will consider the quantum link inspired truncation where the original operator algebra is replaced by a finite spin-s representation with

$$L \to L^3, \ \mathrm{e}^{\pm i\hat{\theta}} \to L^{\pm} \ , \quad (4)$$

and $|n| \leq s$.

We now discuss the time continuum limit and the finite spin projection by computing the transfer matrix using the TRG method. Following the procedure described in Refs. [13–15], we can write

$$Z = \mathrm{Tr} \prod_{(x,t)} T^{(x,t)}_{n_x n'_x n_t n'_t} \ , \quad (5)$$

with the local tensor expressed in terms of the modified Bessel functions:

$$T^{(x,t)}_{n_x n_{x'} n_t n_{t'}} = \sqrt{I_{n_t}(\beta_t) I_{n_{t'}}(\beta_t) \exp(\mu(n_t + n'_t))} \sqrt{I_{n_x}(\beta_s) I_{n_{x'}}(\beta_s)} \delta_{n_x + n_t, n_{x'} + n_{t'}} \ . \quad (6)$$

The indices n_x, n'_x, n_t and n'_t label the four links coming out of (x,t) in the x and t direction and the trace Tr refers to the sum over all these link indices. We can now consider a time slice at a given t and perform the traces over the space links. This defines a transfer matrix

$$\mathbb{T}_{(n_1, n_2, \ldots n_{N_x})(n'_1, n'_2, \ldots n'_{N_x})} = \sum_{n_{x1} n_{x2} \ldots n_{N_x}} T^{(1,t)}_{n_{xN_x} n_{x1} n_1 n'_1} T^{(2,t)}_{n_{x1} n_{x2} n_2 n'_2 \ldots} \ldots T^{(N_x,t)}_{n_{x(N_x-1)} n_{xN_x} n_{N_x} n'_{N_x}} \ . \quad (7)$$

The indices $(n_1, n_2, \ldots n_{N_x})$ represent the past and $(n'_1, n'_2 \ldots n'_{N_x})$ the future and can be interpreted as the two indices of the transfer matrix. We can write

$$Z = \mathrm{Tr} \mathbb{T}^{N_t} \ . \quad (8)$$

In view of the rapid decay of the $I_n(\beta)$ when $|n|$ increases at fixed β, good approximations can be obtained by replacing the infinite sums by sums restricted to $-n_{max}$ to n_{max}. We denote the number of states $D_{st} = 2n_{max} + 1$. With this truncation the transfer matrix is a $D_{st}^{N_x} \times D_{st}^{N_x}$ matrix. It is possible to coarse grain the transfer matrix efficiently by using a higher order singular value decomposition (HOTRG) described in [12]. This procedure then reduces the two site transfer matrix to a $D_{st} \times D_{st}$ matrix and thus accomplishes the blocking from two sites to a single site. Note that in the spin-1 truncation, the restriction to dimension 3 is only applied to the initial tensor and we keep D_{st} much larger than 3 as we keep blocking. In other words, the spin projection represents a microscopic modification of the model, while we need to keep D_{st} as large as possible in order to keep a good macroscopic accuracy.

The accuracy of the results depend on D_{st} and can be monitored through its convergence. In the Mott insulating (MI) phase, the ratios of eigenvalues converge very fast and become independent of the volume of the system after a few iterations. Inside the superfluid (SF) phase, the two largest eigenvalues become degenerate and one needs to use larger D_{st} to get comparably accurate results. The details of the convergence, error estimates and ways to improve the accuracy of the transfer matrix method will be documented in a separate paper [25].

We have used the worm algorithm [17, 18] to calculate the particle number density $\langle N \rangle$ as defined in [18] at a few points near the tips of the MI region (where the results of the HOTRG are the least accurate) for a finite volume $(L_x = 16, L_y = 16)$ in order to cross-check the HOTRG results. This comparison is shown in Table I showing that the HOTRG results agree with the worm algorithm's within 1% or less.

β	μ	$\langle N \rangle$ (worm)	$\langle N \rangle$(HOTRG)
1.12	0.01	0.00726(1)	0.00728(8)
0.46	1.8	0.98929(1)	0.9892(3)
0.28	2.85	1.98980(2)	1.989(2)
0.2	3.53	2.96646(3)	2.967(1)
0.12	4.3	3.96206(4)	3.965(1)

TABLE I. Comparison of $\langle N \rangle$ between the worm algorithm and the HOTRG.

By looking at the ratio of the first two eigenvalues (λ_2/λ_1) of the transfer matrix and the particle number density $\langle N \rangle$, the phase diagram of the classical $O(2)$ model in the thermodynamic limit can be obtained for both $\beta_t = \beta_x$ and $\beta_t \gg \beta_x$ cases. In the $\beta_t = \beta_x = \beta$ case, Fig. 1 shows the behavior of the second normalized eigenvalues and the changes in $\langle N \rangle$ with an increase in μ for small β. The system reaches the SF phase when $\lambda_2/\lambda_1 = 1$. Correspondingly, there is a jump in the particle number density between two adjacent integers which stand for two different MI phases. The fact that the system goes through the MI and SF phase alternately as one

increases μ is shown in the β-μ phase diagram shown in Fig. 2 (top).

The spin-1 projection is also shown in these figures. When μ is not too large, only small differences with the original, unprojected model are observed. However, when μ becomes large enough to have $\langle N\rangle > 1$, the truncation prevents such a large occupation and $\langle N\rangle$ saturates to 1 as expected and there is no $\langle N\rangle = 2$ MI phase. The phase separation lines (Figs. 2 and 3) separating the MI $\langle N\rangle = 0$ phase from the SF phase approximately coincides with the line for the model with an infinite number of states. Similarly, the spin-2 projection reproduces well the $\langle N\rangle = 0$ and 1 boundaries while discrepancies appear for $\langle N\rangle = 2$.

In the limit where the interactions among the spatial sites are negligible, the problem reduces to a one site problem (simple quantum mechanics) as in mean field theory [19]. In this limit, the average occupation per site n is obtained by maximizing $I_n(\beta_t)e^{n\mu}$. In the limit of large β_t for the time continuum limit, this implies that the jumps in n occur at integer values of $\beta_t\mu - 1/2$. In the limit of small $\beta_t = \beta_x$ for the isotropic case, this implies that the jumps occur at integer values of $\beta e^{\mu}/2$. Changing the vertical coordinate by $\mu \to \beta e^{\mu}/2$, the shape of the phase diagram of the isotropic system looks like the cuspy shapes found for the Bose-Hubbard in one spatial dimension [20, 21] (see Fig. 2 (bottom)). In the continuum time limit ($\beta_t \gg \beta_x$), by defining the effective chemical potential $\mu_e = \mu\beta_t - 1/2$ and effective coupling $\beta_e = \beta_x\beta_t$, we find that the same MI-SF pattern appears in the β_e-μ_e plane (Fig. 3).

Optical lattices provide accurate quantum simulators for the Bose-Hubbard model [26]. Interpreting the positive (negative) eigenvalues of L as the charges of particles (antiparticles) states associated with a complex scalar field, it is natural to consider a two-species Bose-Hubbard Hamiltonian on a lattice. We use the following parameterization:

$$\mathcal{H} = -\sum_{\langle xy\rangle}(t_a a_x^\dagger a_y + t_b b_x^\dagger b_y + h.c.) - \sum_{x,\alpha}(\mu + \Delta_\alpha)n_x^\alpha + \sum_{x,\alpha}\frac{U_\alpha}{2}n_x^\alpha(n_x^\alpha - 1) + W\sum_x n_x^a n_x^b + \sum_{\langle xy\rangle,\alpha} V_\alpha n_x^\alpha n_y^\alpha \tag{9}$$

with $\alpha = a, b$ indicating the two different species, $n_x^a = a_x^\dagger a_x$ and $n_x^b = b_x^\dagger b_x$ the number operators, and $|n_x^a, n_x^b\rangle$ the corresponding on-site basis. This class of models has been studied extensively [27–30]. It is possible to adjust the chemical potentials in order to set $\langle n_x\rangle = \langle n_x^a + n_x^b\rangle = 2$. In the limit where $U_a = U_b = W$ are very large and positive, the on-site Hilbert space can then be restricted to the states satisfying $n_x = 2$ at each site. All the other states (with $n_x \neq 2$) belong to high-energy sectors that are separated from this one by energies of order U. The three states $|2,0\rangle$, $|1,1\rangle$ and $|0,2\rangle$ correspond to the three states of the spin-1 projection considered above. Going back to the general Hamiltonian (Eq. 9), we write $U_{a(b)} = U \pm \delta$ and assume $U \gg \delta, (U-W), V, t_\alpha, \Delta_\alpha$ and do degenerate perturbation theory. Virtual processes exchanging particles between neighboring sites are allowed at second order with contributions proportional to $-t_\alpha t_{\alpha'}/U$. The hopping amplitude is tunable and when chosen to be $t_\alpha = \sqrt{V_\alpha U}$, the final result is that the effective Hamiltonian up to second order in degenerate perturbation theory corresponds to the spin-1 projection of the rotor Hamiltonian of Eq. (3) with $\tilde{J} = \sqrt{V_a V_b}$, $\tilde{U} = 2(U-W)$, and $\tilde{\mu} = (\Delta_a + 5V_a) - (\Delta_b + 5V_b)$. Similarly, by increasing the chemical potentials, it is possible to restrict the Hilbert space to $n_x^a + n_x^b = 2s$ which corresponds to a spin-s projection in the $O(2)$ model.

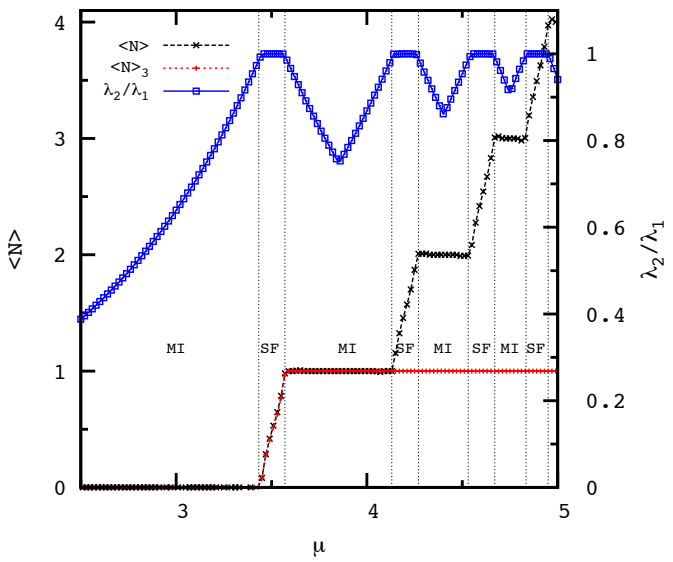

FIG. 1. The second normalized eigenvalues (λ_2/λ_1) of the transfer matrix and the particle number density $\langle N\rangle$ at $\beta = 0.06$ from HOTRG calculation with the number of states $D_{st} = 15$ are shown for the 1+1 D $O(2)$ model. As a comparison, the particle number density $\langle N\rangle_3$ for the spin-1 projection (3-states) is also shown.

This two-species Bose-Hubbard model can be realized in a ^{87}Rb and ^{41}K Bose-Bose mixture where an interspecies Feshbach resonance is accessible [31, 32]. Due to the physical nature of the different atoms, the hopping amplitudes (t_a, t_b) are different to begin with, as well as the intraspecies interactions. In addition, species-dependent optical lattices [33–37] are widely used in boson systems, which allows the hopping amplitudes of each individual species to be further tuned to the desired value. As mentioned above, the interspecies interaction (W) can be controlled by an external magnetic field [32]. Finally, the extended repulsion, V_α, is present and small when we consider Wannier Gaussian wave functions centered on nearby lattice sites according to previous study

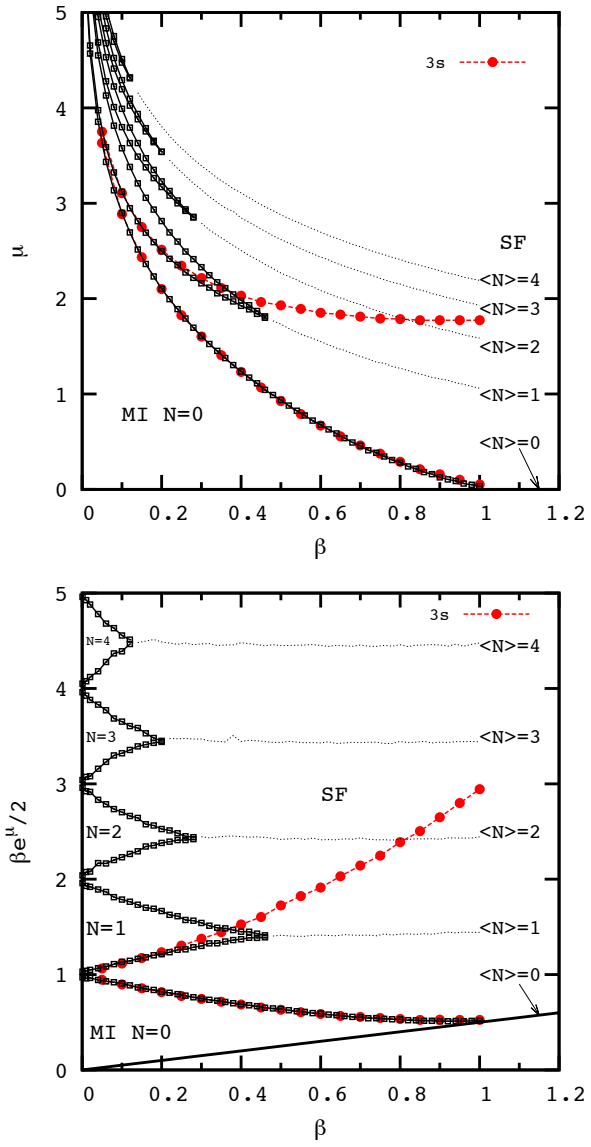

FIG. 2. Top: The phase diagram for the 1+1 D $O(2)$ model in the β-μ plane. Bottom: The phase diagram in the β-$\beta e^{\mu}/2$ plane. $\langle N\rangle = 0$ ($\mu = 0$) line in the SF phase is the Kosterlitz-Thouless phase in the 1+1 D $O(2)$ model at $\mu = 0$. In both graphs, the lines labeled by "3s" stand for the phase separation lines of the spin-1 (3-states) system.

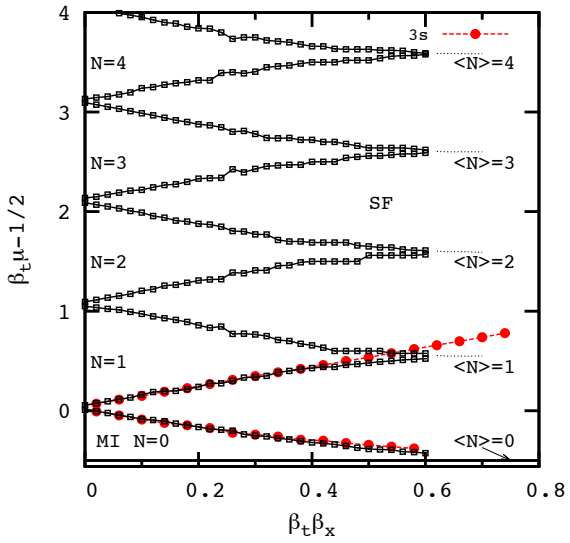

FIG. 3. Phase diagram for the 1+1 D $O(2)$ model at $\beta_t = 10$ in β_e-μ_e plane is shown. The lines labeled by "3s" stand for the phase separation lines of the spin-1 (3-state) system.

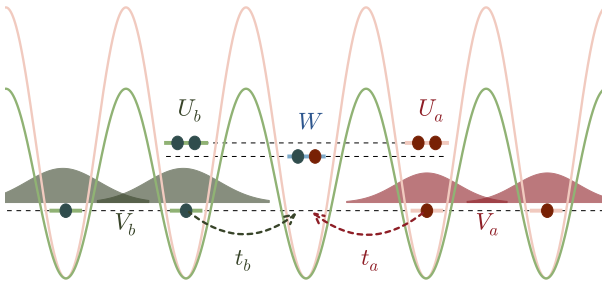

FIG. 4. (Color Online) Two-species (green and red) of bosons on species-dependent optical lattices (with the same color). The nearest neighbor interaction is coming from the overlap of Wannier Gaussian wave functions. We assume the difference between intra-species interactions are small $U \gg \delta$.

[38]. This is schematically illustrated in Fig. 4. This may be the most difficult parameter to achieve, but other proposals may be explored, such as by using dipolar bosons [39], or by pumping bosons to higher Bloch bands [40] in order to engineer the nearest neighbor interaction.

In summary, we have proposed steps connecting a classical model having common features with those considered in lattice gauge theory to physical models potentially implementable on optical lattices and evolving at physical time. We have demonstrated that the TRG method is developing into a robust tool complementing traditional MC methods. A first test of the correspondence would be to check that the Bose-Hubbard model reproduces the phase diagram of Fig. 3 and the spectrum as calculated with the TRG. In LGT calculations, important information regarding the spectrum and matrix elements can be extracted from the 2 and 3 point functions obtained by introducing localized sources. Techniques to gather related information from an optical lattice system remain to be developed. The ultimate goal is to obtain the quantitative information directly from the optical lattice system which could be considered as a way to do quantum computing.

Acknowledgments. We thank Masanori Hanada, Peter Orland, Lode Pollet, Boris Svistunov, the partici-

pants of the Math-Physics and Particle and Nuclear Seminar at the University of Iowa and of SIGN 2014 for stimulating discussions. This research was supported in part by the Department of Energy under Award Numbers DOE grant DE-FG02-05ER41368, de-sc0010114 and DE-FG02-91ER40664, and by the Army Research Office of the Department of Defense under Award Number W911NF-13-1-0119. Part of the simulations were done at CU Boulder Janus clusters and Y. L. thanks D. Mohler and J. Simone for in-sightful discussions on code development.

[1] D. Banerjee, M. Bögli, M. Dalmonte, E. Rico, P. Stebler, U.-J. Wiese, and P. Zoller, Phys. Rev. Lett. **110**, 125303 (Mar 2013)
[2] E. Zohar, J. I. Cirac, and B. Reznik, Phys. Rev. Lett. **110**, 125304 (Mar 2013)
[3] L. Tagliacozzo, A. Celi, A. Zamora, and M. Lewenstein, Annals of Physics **330**, 160 (2013), ISSN 0003-4916
[4] Y. Liu, Y. Meurice, and S.-W. Tsai, PoS **LATTICE2012**, 246 (2012), arXiv:1211.4126 [hep-lat]
[5] For a recent review and additional references see: U. J. Wiese(2013), arXiv:1305.1602 [quant-ph]
[6] J. Kogut and L. Susskind, Phys. Rev. D **11**, 395 (Jan 1975)
[7] T. Banks, L. Susskind, and J. Kogut, Phys. Rev. D **13**, 1043 (Feb 1976)
[8] E. Fradkin and L. Susskind, Phys. Rev. D **17**, 2637 (May 1978)
[9] J. B. Kogut, Rev. Mod. Phys. **51**, 659 (Oct 1979)
[10] P. Orland and D. Rohrlich, Nucl.Phys. **B338**, 647 (1990)
[11] S. Chandrasekharan and U. Wiese, Nucl.Phys. **B492**, 455 (1997), arXiv:hep-lat/9609042 [hep-lat]
[12] Z. Y. Xie, J. Chen, M. P. Qin, J. W. Zhu, L. P. Yang, and T. Xiang, Phys. Rev. B **86**, 045139 (Jul 2012)
[13] Y. Liu, Y. Meurice, M. P. Qin, J. Unmuth-Yockey, T. Xiang, Z. Y. Xie, J. F. Yu, and H. Zou, Phys. Rev. D **88**, 056005 (Sep 2013)
[14] A. Denbleyker, Y. Liu, Y. Meurice, M. P. Qin, T. Xiang, Z. Y. Xie, J. F. Yu, and H. Zou, Phys. Rev. D **89**, 016008 (Jan 2014)
[15] J. F. Yu, Z. Y. Xie, Y. Meurice, Y. Liu, A. Denbleyker, H. Zou, M. P. Qin, J. Chen, and T. Xiang, Phys. Rev. E **89**, 013308 (Jan 2014)
[16] P. Hasenfratz and F. Karsch, Phys.Lett. **B125**, 308 (1983)
[17] N. Prokof'ev and B. Svistunov, Phys. Rev. Lett. **87**, 160601 (Sep 2001)
[18] D. Banerjee and S. Chandrasekharan, Phys.Rev. **D81**, 125007 (2010), arXiv:1001.3648 [hep-lat]
[19] M. P. A. Fisher, P. B. Weichman, G. Grinstein, and D. S. Fisher, Phys. Rev. B **40**, 546 (Jul 1989)
[20] G. G. Batrouni and R. T. Scalettar, Phys. Rev. B **46**, 9051 (Oct 1992)
[21] T. D. Kühner and H. Monien, Phys. Rev. B **58**, R14741 (Dec 1998)
[22] A. M. Polyakov, *Gauge Fields and Strings* (Harwood, Chur, Switzerland, 1987)
[23] M. P. A. Fisher, *Strong Interaction in Low Dimensions* (Kluwer Academic, 2004) Chap. Duality in low dimensional quantum field theories
[24] S. Sachdev, *Quantum Phase Transitions*, Second ed. ed. (Cambridge University Press, 2011) ISBN 9780521514682
[25] H. Zou, Y. Liu, S. Chandrasekharan, J. Unmuth-Yockey, Z. Y. Xie, T. Xiang, and Y. Meurice, "A tensor renormalization approach of the $O(2)$ model with a chemical potential," Preprint in preparation
[26] S. Trotzky, L. Pollet, F. Gerbier, U. Schnorrberger, I. Bloch, N. V. Prokof'Ev, B. Svistunov, and M. Troyer, Nature Physics **6**, 998 (Dec. 2010), arXiv:0905.4882 [cond-mat.quant-gas]
[27] A. B. Kuklov and B. V. Svistunov, Phys. Rev. Lett. **90**, 100401 (Mar. 2003)
[28] A. Kuklov, N. Prokof'ev, and B. Svistunov, Phys. Rev. Lett. **92**, 050402 (Feb. 2004)
[29] P. Chen and M.-F. Yang, Phys. Rev. B **82**, 180510 (Nov. 2010)
[30] C.-M. Chung, S. Fang, and P. Chen, Phys. Rev. B **85**, 214513 (Jun. 2012)
[31] J. Catani, L. De Sarlo, G. Barontini, F. Minardi, and M. Inguscio, Phys. Rev. A **77**, 011603 (Jan. 2008)
[32] G. Thalhammer, G. Barontini, L. De Sarlo, J. Catani, F. Minardi, and M. Inguscio, Phys. Rev. Lett. **100**, 210402 (May 2008)
[33] P. Lee, M. Anderlini, B. Brown, J. Sebby-Strabley, W. Phillips, and J. Porto, Phys. Rev. Lett. **99**, 020402 (Jul. 2007)
[34] M. Anderlini, P. J. Lee, B. L. Brown, J. Sebby-Strabley, W. D. Phillips, and J. Porto, Nature **448**, 452 (Jul. 2007)
[35] D. McKay and B. DeMarco, New J. Phys. **12**, 055013 (May 2010)
[36] P. Soltan-Panahi, J. Struck, P. Hauke, A. Bick, W. Plenkers, G. Meineke, C. Becker, P. Windpassinger, M. Lewenstein, and K. Sengstock, Nat Phys **7**, 434 (May 2011)
[37] N. Belmechri, L. Förster, W. Alt, A. Widera, D. Meschede, and A. Alberti, J. Phys. B: At. Mol. Opt. Phys. **46**, 104006 (May 2013)
[38] G. Mazzarella, S. Giampaolo, and F. Illuminati, Phys. Rev. A **73**, 013625 (Jan. 2006)
[39] C. Trefzger, C. Menotti, and M. Lewenstein, Phys. Rev. Lett. **103**, 035304 (Jul. 2009)
[40] V. W. Scarola and S. D. Sarma, Phys. Rev. Lett. **95**, 033003 (2005)